Hindawi
Advances in Civil Engineering
Volume 2022, Article ID 8102488, 15 pages
https://doi.org/10.1155/2022/8102488

Research Article

Research on the Reuse of Discharged Soil from EBP Shield Tunnels in Synchronous Grouting Material

Guijun Luo,[1] Chao Xiao ,[1] Yuan Liu,[2] Kejun Feng,[2] and Qingguo Ren[1]

[1]*CCFED Civil Engineering Co., Ltd., Changsha 410004, China*
[2]*Hunan University, Changsha 410082, China*

Correspondence should be addressed to Chao Xiao; xiaochao317@qq.com

Received 7 November 2021; Accepted 10 December 2021; Published 10 January 2022

Academic Editor: Yu Liang

Great practical significance and engineering application value can be achieved when the large amount of discharged soil produced by EPB shield tunnels is recycled and comprehensively utilized. As one of the key processes of shield construction, synchronous grouting needs a large amount of bentonite, cement, fly ash, sand, and other materials. The research on the reuse of shield muck as synchronous grouting material is carried out based on Zhengzhou subway project. The physical properties and phase of the discharged soil from EPB shield tunnels are studied by using laboratory tests and XRD. The statistics show that the shield muck meets the performance requirements of bentonite and fine sand in synchronous grouting materials. The optimal grout ratio of the reused muck is obtained based on the optimization idea of multiobjective programming by MATLAB. Considering the combined effect of seepage field, stress field, and the timeliness of the grout, the influences of grouting pressure and the filling rate of synchronous grouting on surface settlement, plastic zone of strata, and segment deformation are analyzed by using finite difference method. The results prove that the surface settlement and segment deformation can be better controlled when the grouting pressure is at 0.18 MPa and the grouting rate is at 120%–150%.

1. Introduction

EPB shield method has become the most widely used construction method in urban subway construction in China. A large amount of muck is generated during shield construction. The shield muck not only occupies a large amount of land, reduces soil quality, and affects air and water quality but also has certain security risks. Besides, it is expensive to transport the muck directly to waste disposal area. Therefore, the research on the reuse of shield muck is of great practical significance and practical value.

Presently, some researches on the reuse of shield muck have been carried out, including the following aspects: (1) engineering grout treatment technology. Zha et al. [1] studied a formula for converting wastewater-based drilling fluid into environmentally friendly soil. The treatment process can achieve harmless treatment and effective utilization of drilling waste. Through data analysis of the unconfined compressive strength, triaxial compressive strength, indirect tensile strength, humidity sensitivity, and seismic modulus, Shon et al. [2] conclude that it is feasible to use modified drilling waste as a basic material for road construction. Whitaker et al. [3] studied the effects of drilling mud application rate on soil salt accumulation and leaching, and the effects of applying time and rate of the drilling mud on wheat production are discussed. Dong [4] studied the treatment technology on drilling mud and explored the solidification treatment technology on drilling waste through laboratory research. Peng et al. [5] systematically analyzed and studied several main harmless treatment methods (solidification treatment, secondary utilization of waste grout) in China. (2) Reuse of shield muck: through the treatment process of grout in Weser river tunnel excavation, Grohs [6] found that the separated sand can be used as the load-bearing layer, sound insulation wall's cover layer, and filling material of highway subgrade according to the different particle content. Zhong et al. [7] studied the reuse of excavated silty fine sand in shield synchronous grouting. He

et al. [8] used shield muck sand (modulus at 1.88) from Shuangdun Station to Wangjiadun Center Station of Wuhan Metro Line 3 as fine aggregate to prepare environmentally friendly single-liquid synchronous grouting material with high performance through optimizing experimental mix proportion. In summary, although scholars have achieved fruitful results in the reuse of shield muck, there are few studies on the reuse of EPB shield muck as synchronous grouting material, and systematic research results have not been reported. Synchronous grouting is one of the key links in shield construction. Usually, grout is injected into the gaps between shield tail and segment to fill the gap and control strata deformation [9–12]. At the same time, the grouting protection layer is formed around the tunnel to improve the impermeability of shield tunnel [13–15]. The stratum that the shield passes through is usually soft soil stratum containing lots of clay particles and fine sand. If proper treatment is carried out, the discharged soil is one of the high quality raw materials for synchronous grouting.

In view of this, based on the construction example of a section crossing silty clay stratum and clayey silt stratum with sandy silt in Zhengzhou Metro, this paper discusses the feasibility about the reuse of shield muck, and the best synchronous grouting proportion with the reused shield muck is obtained. Moreover, the influences of grouting pressure and filling rate on surface settlement, soil plastic zone, and segment deformation are studied. The research results are expected to provide reference for similar projects.

2. Project Overview

The main strata of a certain section of Zhengzhou Metro are clayey silt stratum with sandy silt, and the local strata are silty clay stratum and clayey silt stratum with sandy silt. According to geological prospecting, 56% of the strata traversed by the tunnel are silty clay, 38% are fine sand, and 6% are silty clay mixed with sandy silt, as shown in Figure 1.

Two Earth pressure balance shield machines with a diameter of 6250 mm were used for construction. Reinforced concrete segments are used as tunnel lining. The segment has an outer diameter of 6.2 m, a thickness of 0.35 m, and a width of 1.5 m. The theoretical muck output per ring is 49.4 m^3. The theoretical grouting volume per ring is 4.1 m^3, and the filling factor is 1.5–2.0.

3. Feasibility of Shield Muck as Grouting Material

3.1. Engineering Features Test of the Shield Muck. The detailed composition and phase analysis of shield muck, mainly including density, water content, specific gravity, limit moisture content, void ratio, saturation, and grading feature and other physical characteristics tests, are carried out. Shield muck sample is shown in Figure 2.

3.1.1. Basic Physical Properties. Basic physical properties of shield muck can be obtained by physical property measurement, and the results are listed in Table 1.

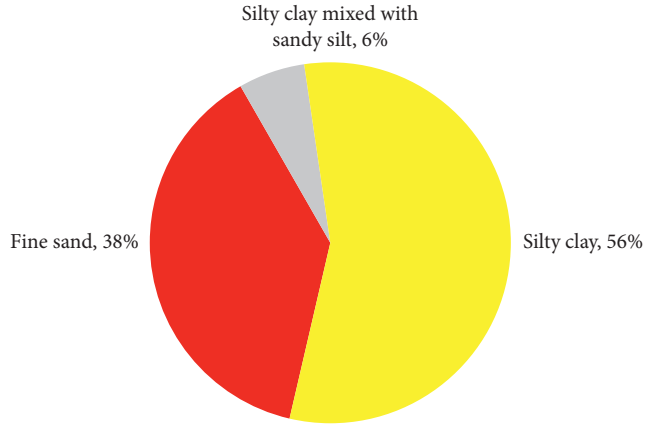

Figure 1: The proportion of strata that the shield crosses.

According to the measurement results, the muck sample has moderate moisture content and a viscosity index of 0.5. The soil sample is a low-liquid limit silty clay in a plastic state.

3.1.2. Grading Curve of the Muck. In the analysis of particle size composition, the particle size distribution of soil above 0.075 mm was determined by sieving method, and the particle size distribution of soil below 0.075 mm was measured by densimeter method considering the existence of fine particles in the muck of silty clay. The particle size composition of the muck is manifested in Table 2. The grading curve is portrayed in Figure 3.

According to Table 2 and Figure 3, the particle size distribution of silty clay samples is uneven, and the particle gradation is good. There are a lot of fine particles in the sample. The fine particles with particle size less than 0.075 mm account for 39.32%, and the clay particles with particle size less than 0.005 mm account for 8.45%.

Only the sieving method is used to determine the particle size distribution, and the fineness modulus and mud content are used to evaluate the quality of sand samples in the analysis of particle size composition of fine sand in muck. The particle size composition of the fine sand in muck is shown in Table 3, and the gradation curve is demonstrated in Figure 4.

According to Table 3 and Figure 4, the particle size distribution of fine sand samples is uniform and poor, mostly in the range of 0.6–0.15, and the composition is mostly composed of medium sand and fine sand.

3.1.3. Mineral Composition Analysis of the Muck. Multipurpose X-ray diffractometer (XRD) is applied to analyze the phase of silty clay and fine sand. The mineral composition of silty clay in muck is mainly composed of quartz (21.35%), feldspar (16.38%), and montmorillonite (31.03%). The mineral composition of fine sand mainly consists of quartz (35.03%) and feldspar (27.35%).

3.2. Feasibility Analysis of Shield Muck as Grouting Material. The clay mineral composition of the silty clay in muck is high with favorable water absorption and expansion properties.

(a) (b)

Figure 2: Shield muck sample: (a) fine sand, (b) silty clay.

Table 1: Basic physical properties of shield muck.

Soil sample	Water content (%)	Wet density (g)	Dry density (g)	Specific gravity	Plasticity limit (%)	Liquid limit (%)	Plasticity index	Void ratio	Degree of saturation
Silty clay	18.76	2.055	1.722	2.634	13.25	24.468	11.218	0.788	63.3
Fine sand	4.83	1.928	1.836	—	—	—	—	—	—

Table 2: Particle size composition of silty clay in muck.

Sample name	Contents of particles smaller than a certain size (mm) (%)						Uniformity coefficient	Curvature coefficient
	1	0.25	0.075	0.01	0.005	0.001		
Silty clay	94.68	69.46	39.32	11.63	8.45	3.56	26.00	1.73

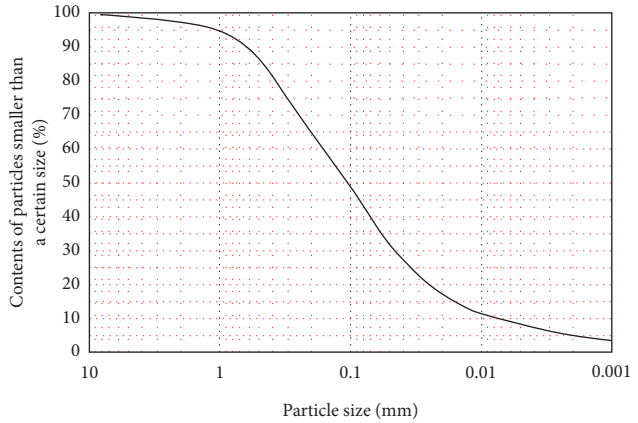

Figure 3: Grading curve of silty clay in muck.

Table 3: Particle size composition of fine sand in muck.

Sample name	Contents of particles smaller than a certain size (mm) (%)						Fineness modulus	Mud content (%)
	4.75	2.36	1.18	0.6	0.3	0.15		
Fine sand	99.86	99.25	98.05	91.15	42.99	9.36	1.61	9.11

Besides, the particle size of soil sample is small, and the specific surface area of soil particles per unit mass is large, which can effectively improve the viscosity and stability of the grouting liquid. Therefore, it is feasible to replace the bentonite in the raw materials of synchronous grouting liquid based on the features like physical properties, mineral composition, and particle size composition of the muck in the section of Zhengzhou Metro. Moreover, the mineral

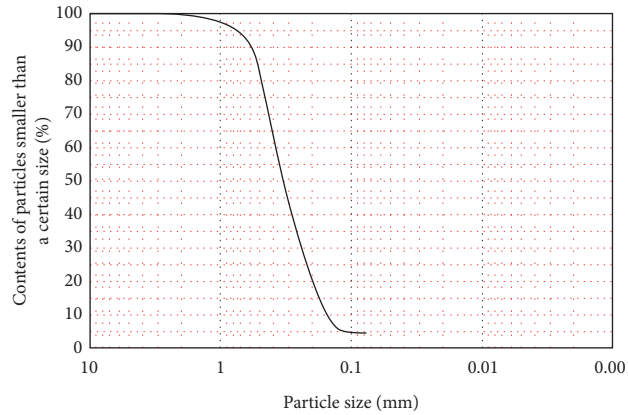

Figure 4: Grading curve of fine sand in muck.

components of the fine sand in muck are mainly quartz and feldspar with little mud content. It has the basic conditions for recycling and the utilization as engineering sand, so it is feasible to replace the fine sand in the raw materials of synchronous grouting liquid.

4. Optimization of Ratio of the Reused Muck Grout

Based on the engineering situation of the shield section, cement, fly ash, silty clay in muck (substitute for bentonite), fine sand in muck (substitute for river sand), bentonite, and water are chosen as single-liquid grouting materials with active cement mortar.

By using the basic theory and method of uniform design, a large number of tests can be effectively avoided. Uniform design was initiated by Chinese statistician Professor Fang Kaitai and member of Chinese Academy of Sciences Wang Yuan, and it is the premier method to conduct multifactor and multilevel experimental design. It can complete the research and development of complex scientific research projects and new products with fewer experiments. The biggest feature is that the number of experiments can be equal to the maximum level number, rather than the square of the number of experimental factors. Moreover, the number of experiments is only related to the number of factors to be investigated. However, the number of trials should be about 3 times the number of experimental factors, which is conducive to modeling and optimization.

The synchronous grouting liquid is a kind of hard single liquid, and its influencing factors can be generally divided into four properties, namely, water-binder ratio, binder-sand ratio, bentonite-water ratio, and fly ash-cement ratio. The water-binder ratio is the ratio of water to cementitious materials. The bentonite-water ratio is the ratio of bentonite to water. The cement-sand ratio is the ratio of cementitious materials to the sand. The fly ash-cement ratio is the ratio of fly ash to cement. To analyze the influence of each influencing factor on the construction performance of the grout and design the optimal mix proportions, five levels of tests were set for each influencing factor, and the number of tests was three times the actual level of the test. Therefore, 15 groups of tests were arranged, namely, the uniform design of 4 factors and 15 levels. Referring to Appendix I of Fang Kaitai's *uniform design and uniform design table* [16], the uniform design was carried out by choosing columns 1, 2, 4, and 6 of U15 $*$ (157). The material proportions of the uniform design are listed in Table 4. The items of the grouting material performance test mainly include specific gravity test, consistency test, fluidity test, bleeding rate test, setting time test, stone shrinkage test, and unconfined compression test. The test results are presented in Table 5.

Based on the results of uniform test, SPSS software was used for regression analysis with regression method, and quadratic multiple regression model was adopted to analyze the interaction among variables.

$$y = b_0 + \sum_{k=1}^{5} b_k x_k + \sum_{j=1}^{5} \sum_{k=j}^{5} b_{jk} x_j x_k + \varepsilon, \quad (1)$$

where x_i and x_k are test factors, b_0, b_k, and b_{jk} are coregression coefficients, x_1 is the water-binder ratio, x_2 is the binder-sand ratio, x_3 is the bentonite-water ratio, and x_4 is the fly ash-cement ratio. The regression equation of each factor is obtained according to the test results.

Based on the results of regression analysis, each influencing factor of grouting material and each performance of grout are analyzed. The factor was changed within its value range, and the influences of this factor on the specific gravity of mortar, stone shrinkage rate, initial fluidity, 3 h bleeding rate, setting time, and compressive strength are studied. Simultaneously, the range of independent variables in the multiobjective programming problem is determined according to the level interval of uniform test factors, and the fmincon function in MATLAB optimization toolkit is used to solve the multiobjective programming problem with ideal point method. The optimal proportions of synchronous grouting material prepared from shield muck are listed in Table 6. The performances of the grouting material with the optimal proportion are listed in Table 7.

Table 4: Material proportions of uniform experimental design (6.5 kg for each group).

Number	Ratio					
	C (cement) (kg)	F (fly ash) (kg)	S (sand in muck) (kg)	B (silty clay in muck) (kg)	W (water) (kg)	Ratio (C : F: S : B: W)
1	0.558	1.675	2.659	0.268	1.340	1 : 3: 4.76 : 0.48 : 2.4
2	0.420	1.765	2.601	0.184	1.530	1 : 4.2 : 6.19 : 0.44 : 3.64
3	0.626	1.502	2.533	0.136	1.702	1 : 2.4 : 4.05 : 0.22 : 2.72
4	0.420	1.513	2.479	0.348	1.740	1 : 3.6 : 5.9 : 0.83 : 4.14
5	0.674	1.214	2.421	0.302	1.888	1 : 1.8 : 3.6 : 0.45 : 2.8
6	0.482	1.736	2.844	0.106	1.331	1 : 3.6 : 5.9 : 0.22 : 2.76
7	0.713	1.283	2.772	0.335	1.397	1 : 1.8 : 3.89 : 0.47 : 1.96
8	0.490	1.470	2.722	0.251	1.568	1 : 3: 5.56 : 0.51 : 3.2
9	0.372	1.562	2.686	0.139	1.741	1 : 4.2 : 7.22 : 0.37 : 4.68
10	0.509	1.222	2.623	0.415	1.731	1 : 2.4 : 5.15 : 0.82 : 3.4
11	0.389	1.635	3.067	0.194	1.215	1 : 4.2 : 7.88 : 0.5 : 3.12
12	0.579	1.391	2.985	0.165	1.379	1 : 2.4 : 5.15 : 0.29 : 2.38
13	0.386	1.390	2.961	0.341	1.421	1 : 3.6 : 7.67 : 0.88 : 3.68
14	0.620	1.115	2.891	0.312	1.561	1 : 1.8 : 4.67 : 0.5 : 2.52
15	0.429	1.287	2.861	0.206	1.717	1 : 3: 6.67 : 0.48 : 4

Table 5: Test results.

Number	Specific gravity	Stone shrinkage rate (%)			Consistency (cm)	Initial fluidity (cm)	3h bleeding rate (%)	Initial setting time (h)	Compressive strength (MPa)
		1d	7d	28d					7d
1	2.005	3.9	4.1	4.1	13.9	13.8	3.0	8.92	0.81
2	1.878	6.1	6.2	6.2	16.2	21.0	3.0	9.25	0.38
3	1.810	7.2	7.3	7.3	15.2	27.3	5.0	9.93	0.62
4	1.789	8.5	8.7	8.7	13.5	27.0	6.0	21.22	0.30
5	1.720	11.8	12.0	12.0	13.8	26.5	8.0	17.88	0.60
6	1.945	4.2	4.4	4.4	14.1	17.0	3.0	11.58	0.64
7	1.940	4.3	4.4	4.4	12.2	18.0	4.0	9.73	1.01
8	1.825	5.2	5.3	5.3	13.1	22.5	4.0	12.17	0.40
9	1.635	12.4	12.3	12.3	13.0	30.3	12.0	27.95	0.18
10	1.753	10.3	20.5	10.5	13.4	25.5	7.0	17.75	0.36
11	1.925	4.6	4.8	4.8	12.7	17.7	2.0	11.03	0.37
12	1.935	5.7	5.7	5.7	15.0	20.3	3.0	11.42	0.67
13	1.825	6.4	6.5	6.5	13.7	22.3	4.0	15.57	0.32
14	1.783	4.1	4.3	4.3	12.4	15.1	4.0	15.26	0.61
15	1.724	7.1	7.3	7.3	12.7	19.3	6.0	20.13	0.36

Table 6: Optimal proportions of synchronous grouting material prepared from shield muck.

Water-binder ratio	Binder-sand ratio	Bentonite-water ratio	Fly ash-cement ratio	Mass of components per 6.5 kg of grout (kg)				
				Cement	Fly ash	Silty clay in muck	Fine sand in muck	Water
0.74	0.84	0.11	2.75	0.574	1.578	0.184	2.562	1.603

Table 7: Grouting material properties with the optimal proportions.

Specific gravity	Stone shrinkage rate (%)			Initial fluidity (cm)	3h bleeding rate (%)	Initial setting time (h)	Compressive strength (MPa)		
	1d	7d	28d				1d	7d	28d
1.878	5.57	5.77	5.78	22.5	3.6	10	0.62	1.81	5.17

5. Numerical Simulation Research on the Effect of Shield Muck Synchronous Grouting

5.1. Calculation Model and Parameters. The 201 ring to 210 ring of the left line in the interval are used as the test section of muck reuse. The tunnel section at the 205 ring of the left line is chosen as the calculation section to carry out the sensitivity analysis of synchronous grouting construction parameters by using FLAC3D finite difference software. Based on the geological survey data of this project, the main tunneling strata are fine sand and silty clay. The specific stratum parameters are shown in Table 8. The buried depth of underground stable water level is about 16 m, and the tunnel roof is 18 m away from the surface. The distance between the two lines at the section is about 13.5 m. Only the influence of grouting construction in the left line is considered in the calculation considering that the right line has been excavated.

According to the parameters of the shield machine, it can be calculated that the theoretical overbreak gap (25 mm) is half of the difference between the cutter diameter (6480 mm) and the outer diameter of the shield tail. The theoretical gap (70 mm) in shield tail is half of the difference between the inner diameter of the shield tail and the outer diameter of the segment (6200 mm). The theoretical thickness of the ring filled by grout is half of the difference between the cutter diameter and the outer diameter of the segment (140 mm).

Due to the randomness and complexity in the physical and mechanical properties of geotechnical materials, the following calculation conditions and assumptions are used in the numerical simulation: assuming that the thickness of each stratum is uniform and there is no mutual intrusion, surrounding rock and supporting structure are homogeneous and isotropic materials; the strata below groundwater depth are permeable; the water level remains unchanged during tunnel excavation; the grout is incompressible, isotropic, and nondilutable and does not block.

According to the Saint-Venant principle, the displacement and stress changes caused by excavation can be ignored outside the excavation area with 3 to 5 times the tunnel span. Therefore, the left, right, upper, and lower dimensions of the tunnel excavation area are not less than 3–5 times the tunnel span in the actual numerical simulation process. The calculation model is shown in Figure 5. The boundary constraints are the horizontal constraints on the front, back, left, and right of the model, the vertical constraints at the bottom of the model, and the free boundary on the top of the model. For the fluid boundary in seepage, the fluid exchange in the left, right, and bottom boundaries is constrained, and no fluid constraints are imposed on the front and back boundaries.

The stratum soil is simulated with solid element, and it obeys the M-C failure criterion. The shield segment is simulated with solid element, and it conforms to the elastic constitutive model. The segment joint is considered by setting the stiffness reduction coefficient as 0.7. The steel plate of shield machine is simulated by shell element in line with the elastic constitutive model. The grouting layer is simulated by solid element in accordance with elastic constitutive model and is regarded as permeable material. Since the grout is used to fill the gaps between the excavation diameter and the shield body, the filling layer is simulated with solid element with the elastic constitutive model, and it is regarded as impermeable material.

5.2. Simulation Steps of Construction. The calculation steps simulate the three stages of shield construction: (1) shield machine passing stage: the shield shell unit and the overexcavation filling layer in the model are activated; (2) segment out of the shield tail stage: the shield shell element and the overexcavated filling layer are passivated, and the shield tail grouting layer and the segment lining in the model are activated. The grouting pressure of the whole ring in shield tail is applied. Considering the shear movement and consolidation of the grout (the change rate of the grout parameters in the early stage of consolidation is huge), attention should be paid to change the hardening parameters of the grouting layer at the appropriate time and reduce the grouting pressure. (3) Grout hardening stage: time-dependent hardening parameters of grouting layer should also be applied at this stage.

To simulate the field construction more accurately, the three stages of shield construction are divided into six calculation steps (Table 9) according to the hardening process of grouting body considering the construction stage and the influence on surface deformation. In the calculation process, different stratum stress release coefficients are set for different construction steps.

5.3. Calculation of Time-Dependent Parameters of the Grout. To obtain the time-dependent hardening parameters of the materials in this study, the relationships between the elastic modulus and Poisson's ratio of the grout and time are fitted according to the measurement results of the grout performance parameters at different ages, and the relationships are as follows:

$$\begin{aligned} E &= 40 \times \ln(t) + 70, \\ \lambda &= -0.05 \times \ln(t) + 0.38, \end{aligned} \tag{2}$$

where E is elastic modulus, MPa, λ is Poisson's ratio, and t is the curing days of the grout for 0–28 d.

The hardening parameters of the grout are obtained (Table 10) according to the consolidation time point in construction simulation steps 2~6.

5.4. Construction Effect Analysis under Different Grouting Pressure

5.4.1. Range and Vertical Distribution of Grouting Pressure. It is assumed that the grouting pressure and grout are evenly distributed in the whole ring with a diffusion way of filling method. The filling rate of the shield tail void is 100%. To reasonably and fully study the influence of grouting pressure on tunnel structure and surface deformation, the range of

Table 8: Physical mechanics parameters for each stratum of the calculated section.

Stratum name	Permeability coefficient ($cm \cdot s^{-1}$)	Natural unit wet ($kN \cdot m^{-3}$)	Void ratio	Modulus of compression (MPa)	Force of cohesion (kPa)	Angle of friction (°)	Poisson's ratio	Buried depth (m)
Miscellaneous fill	—	18.5	—	5.4	10	15	0.33	0–2.5
Silty sand	—	20.5	—	18	0.1	30	0.25	2.5–7
Clayey silt	0.1	19.6	0.68	6	22.4	19.2	0.30	7–18
Fine sand	10	20.3	0.535	25	0.1	32	0.24	18–22
Silty clay	0.05	20.1	0.639	6.5	32	21	0.32	22–32
Calcareous cemented sandy soil	1.5	21.2	0.4	45	25	36	0.22	32–66

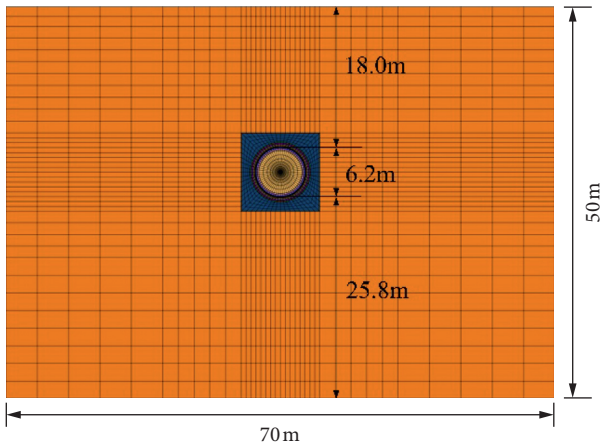

Figure 5: Calculation model.

Table 9: Stratum stress release coefficient at each stage of construction.

Construction simulation steps	1	2	3	4	5	6
Corresponding tunneling stage	Passing stage	Segment off the ring for 0~8h	Segment off the ring for 8~16 h	Segment off the ring for 16~24 h	Grouting hardening for 1~7 d	Grouting hardening for 7~28 d
Settlement stage	Passing settlement	Off-ring settlement			Subsequent settlement	
Release coefficient (%)	15 15	30	25 70	15	10 15	5

Table 10: Hardening parameters of the grout.

Hardening parameters of the grout	Simulation step 2 Off ring for 0~8 h	Simulation step 3 Off ring for 8~16 h	Simulation step 4 Off ring for 16~24 h	Simulation step 5 Off ring for 1~7 d	Simulation step 6 Off ring for 7~28 d
E/MPa	5	15	30	100	200
λ	0.45	0.42	0.37	0.32	0.24
$\rho/kg \cdot m^{-3}$	1900	1900	1900	1900	1900

uniform grouting pressure in the whole ring is set to 0.10 MPa~0.30 MPa, and the linear gradient is 0.04 MPa with a total of 6 working conditions.

Due to the circumferential and longitudinal shear movement of the grout when grouting, and the grout consolidating over time, it is considered that the grouting

pressure is almost reduced to 0 within 1 d after the detachment of the ring (i.e., 9 m away from the shield tail) combined with the engineering practice and literature research. The reduction coefficients of longitudinal grouting pressure are listed in Table 11.

5.4.2. Analysis of Numerical Simulation Results

(1) Surface Settlement. The surface settlement under different grouting pressures is shown in Figure 6. The lateral surface settlement curves under different grouting pressures are basically the same and nearly in line with the characteristics of Gaussian curve. The change of grouting pressure has a great influence on surface settlement. The maximum surface settlement gradually decreases with the increase of grouting pressure, but the width of settlement trough remains unchanged. When the grouting pressure is greater than 0.22 MPa, the uplift occurs at the surface about 25 m away from the axis on both sides of the shield, and the uplift increases with the increase of grouting pressure.

As shown in Figure 7, the segment deforms elliptically and sinks as a whole under the effect of water-soil pressure and grouting pressure. The segment deformation of the feature points changes greatly under different grouting pressure, and the overall settlement of the segment decreases with the increase of grouting pressure. The change values of segment convergence are manifested in Figure 8. With the increase of grouting pressure, the vertical convergence of segment gradually increases, while the horizontal convergence of segment shows a trend of first increasing and then decreasing. When the grouting pressure is set as 0.18 MPa, the horizontal convergence of segment reaches the maximum value of 4.16 mm.

(2) Distribution of Plastic Zone. Table 12 shows the distribution of the soil plastic zone under different grouting pressures. The plastic zone is mainly distributed on both sides of the tunnel, and the size decreases with the increase of grouting pressure. When the value of grouting pressure is less than 0.18 MPa, there are stretched failure units around the tunnel.

The control value of surface settlement in tunnel monitoring project is 10 mm according to the technical specifications of monitoring on urban rail transit engineering and the first-level requirements of engineering monitoring. Figure 6 shows that the minimum grouting pressure is 0.18 MPa. Figure 8 presents that, with the increase of grouting pressure, the convergence of segment clearance gradually increases. Excessive grouting pressure can easily lead to segment dislocation and cracking, so the uniformly distributed grouting pressure in the whole ring should be set to 0.18 MPa.

5.5. Construction Effect Analysis with Different Grouting Quantity

5.5.1. Filling Grouting

(1) Simulation Method. The convergent units are set up in the calculation model in order to simulate the effect that the grout incompletely fills the gaps of the shield tail. As demonstrated in Figure 9, when the segment is just separated from the shield tail, the soil tends to converge to the tunnel. It is assumed that when the grout fills 80% of the shield tail clearance, the remaining 20% is occupied by the convergent soil. To ensure the continuity of the grid in the numerical simulation, the convergent units are used to replace the empty units, and these units are given small strength parameters for approximate simulation.

(2) Working Conditions. Assuming the filling and grouting rate is 80%~100%, the specific conditions are shown in Table 13.

(3) Analysis of Numerical Results

① Surface settlement.

The surface settlement under different backfill grouting conditions is shown in Figure 10. The curves of horizontal surface settlement under different backfill grouting rates are basically the same, which is nearly in line with the feature of Gaussian. The change of backfill grouting rate has a great influence on surface settlement. With the increase of backfill grouting rate, the maximum value of surface settlement decreases gradually, and the variation is considerable. The width of the setting tank remains unchanged when the backfill grouting rate changes.

② Segment deformation.

Figure 11 shows the deformation of segment under different backfill grouting conditions. The segment deforms elliptically and sinks as a whole under the effect of water-soil pressure and grouting pressure. The segment deformation of the feature points changes greatly under different grouting pressure, and the overall settlement of the segment decreases with the increase of grouting pressure.

The relationship between backfill grouting rate and segment convergence is portrayed in Figure 12. With the increase of backfill grouting rate, the vertical convergence and horizontal convergence of the segment show an increasing trend; that is, the ellipticity of segment increases with the increase of backfill grouting rate.

③ Plastic zone distribution.

Table 14 is the distribution of soil plastic zone without backfill grouting. The plastic zone is mainly distributed on the left and right sides of the tunnel, and the size decreases with the increase of filling grouting rate. The plastic deformation areas above the left and right of the tunnel are large when the backfill grouting rate is less than 100%, and it is easy to cause the instability of the soil above the tunnel.

The control value of surface settlement in tunnel monitoring project is 10 mm according to the technical specifications of monitoring on urban rail transit engineering and the first-level requirements of engineering monitoring. Figure 10 shows that when the backfill grouting rate is less than 100%, the maximum surface settlement is greater than 10 mm. Considering the surface settlement and

Table 11: Reduction coefficient of longitudinal grouting pressure.

Construction stage	The circumferential grouting pressure after longitudinal reduction/MPa					Reduction coefficient
Initial grouting pressure	0.1	0.14	0.18	0.22	0.26	0.3
Off ring for 0~8 h	0.08	0.112	0.144	0.176	0.208	0.24
Off ring for 8~16 h	0.04	0.056	0.072	0.088	0.104	0.12
Off ring for 16~24 h	0.02	0.028	0.036	0.044	0.052	0.06

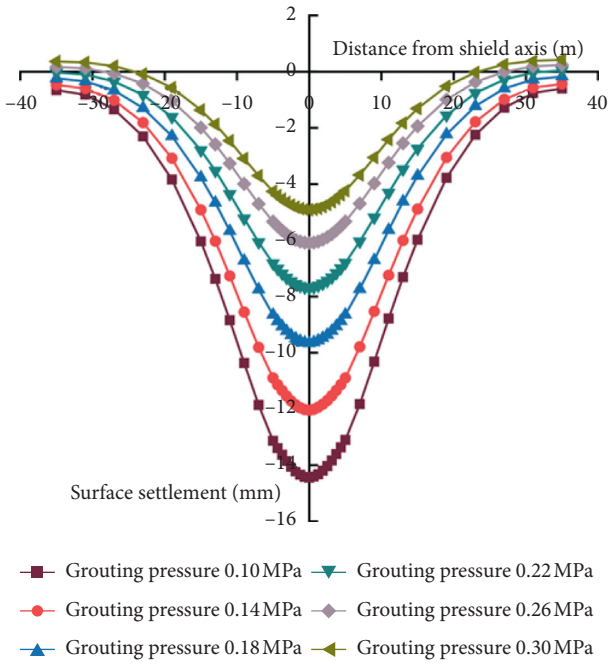

Figure 6: Surface settlement curve under different grouting pressures.

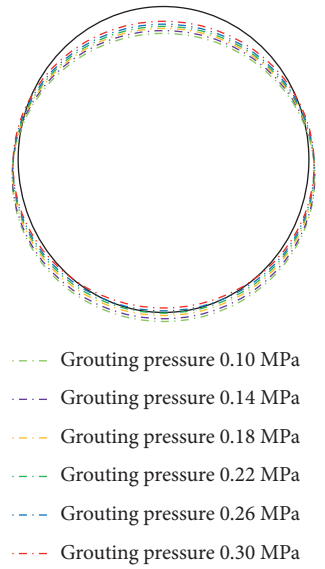

Figure 7: Segment deformation under different grouting pressures.

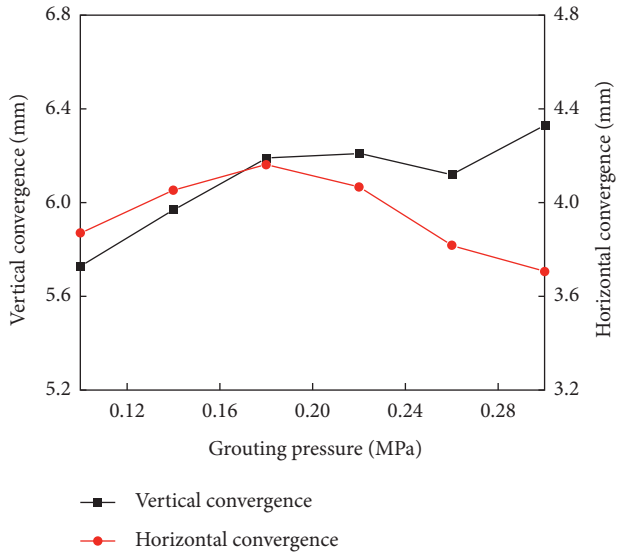

Figure 8: Variation of segment convergence under different grouting pressures.

Table 12: Distribution of plastic zone under different grouting pressures.

Grouting pressure (MPa)	Plastic zone distribution
0.10	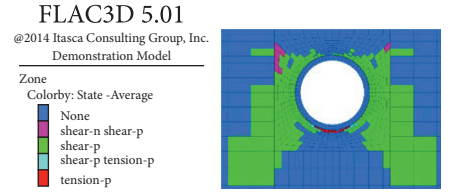
0.14	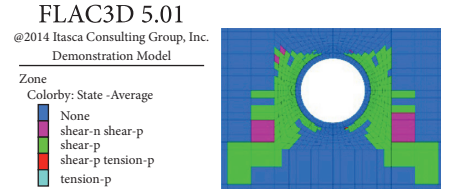
0.18	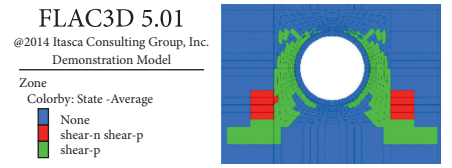
0.22	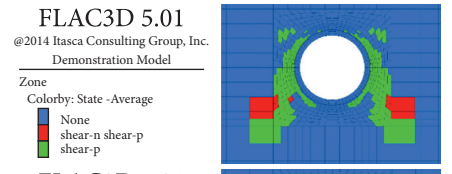
0.26	
0.30	

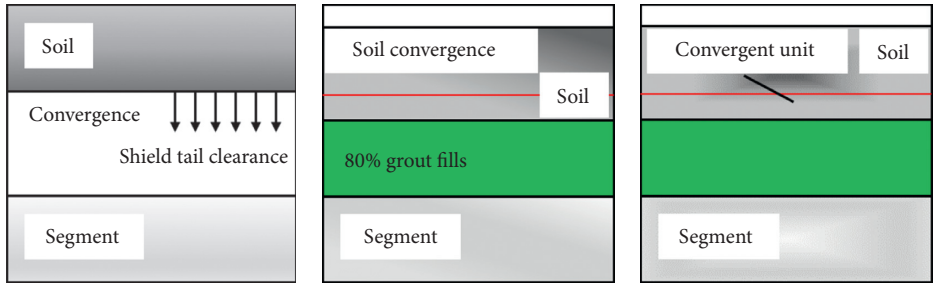

Figure 9: Simulation diagram of grout filling in shield tail gaps. (a) The segment off the ring. (b) Incomplete grout filling. (c) Convergent unit simulation.

Table 13: Conditions of uniform filling grouting.

Uniform grouting pressure on the whole ring/MPa			0.18		
Uniform filling grouting rate/%	80	85	90	95	100

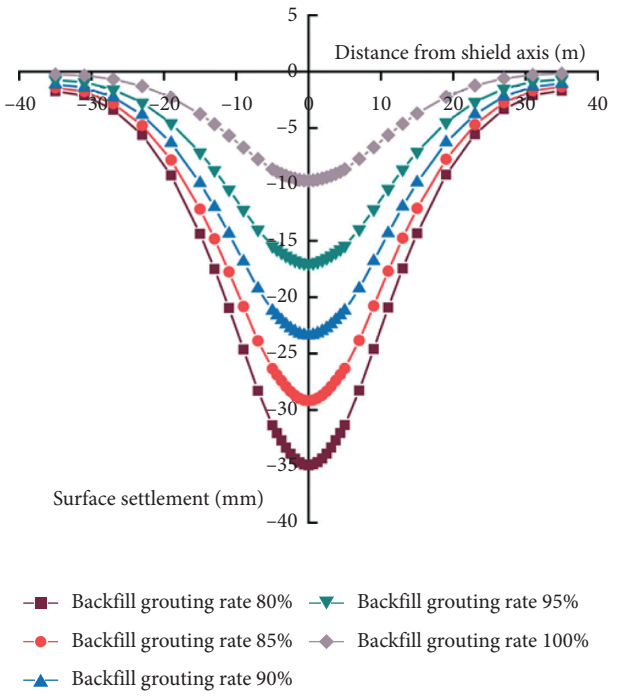

Figure 10: Surface settlement curve under different backfill grouting conditions.

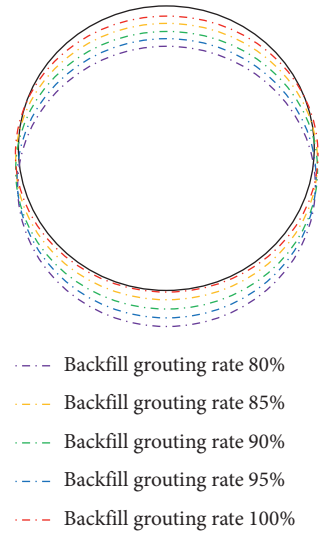

Figure 11: Segment deformation under different backfill grouting conditions.

plastic zone distribution, the backfill grouting rate should be 100%.

5.5.2. Penetration Grouting. The influences of the change of grout injection rate on surface settlement, segment deformation, and plastic zone distribution are simulated simultaneously, and the grout injection rate of 100%–200% is set for calculation and analysis. It is assumed that when the grout injection rate exceeds 100%, penetration grouting happens, and the whole ring is uniformly penetrated. Meanwhile, based on the method in Lei et al. [17], the elastic modulus of grout-soil mixture can be roughly calculated according to (3), and Poisson's ratio is adopted according to grout of corresponding calculation stage. The specific conditions are presented in Table 15.

$$E_3 = E_1 + n_f \times E_2, \tag{3}$$

where E_3 is the elastic modulus of grout-soil mixture, MPa, E_1 is the elastic modulus of the stratum soil where the tunnel is located, MPa, E_2 is the elastic modulus of the corresponding grout, MPa, and n_f is the effective porosity of the soil stratum where the tunnel is located, which is 25.44%.

The simulation results are shown in Figures 13-15. The simulation results indicate that the change of grout injection rate has little effect on surface settlement, segment deformation, and plastic zone distribution. With the increase of grout injection rate, the maximum surface settlement

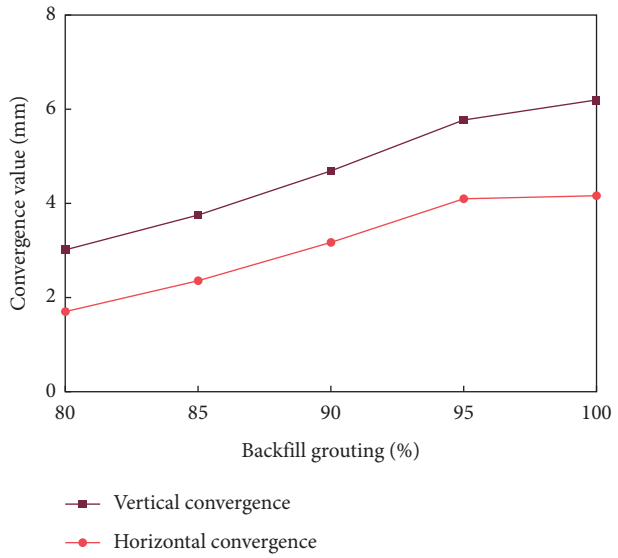

Figure 12: Changes of segment convergence without backfill grouting.

Table 14: Distribution of soil plastic zone without backfill grouting.

Backfill grouting rate (%)	Plastic zone distribution
80	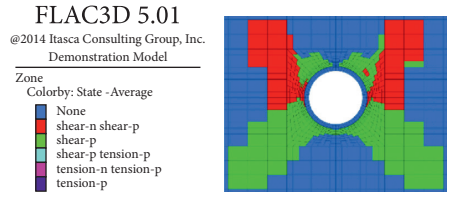
85	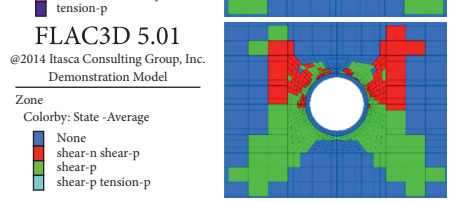
90	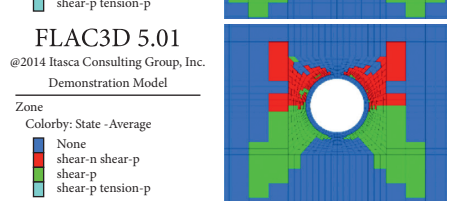
95	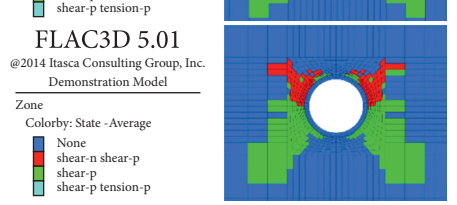
100	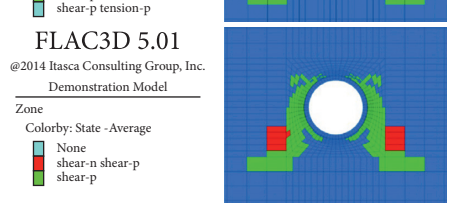

Table 15: Seepage grouting conditions.

Grouting pressure uniformly distributed on the whole ring (MPa)	0.18					
Injection rate of the grout (%)	100	120	140	160	180	200
Thickness of permeable grout-soil mixed layer (m)	0.000	0.106	0.209	0.308	0.405	0.500

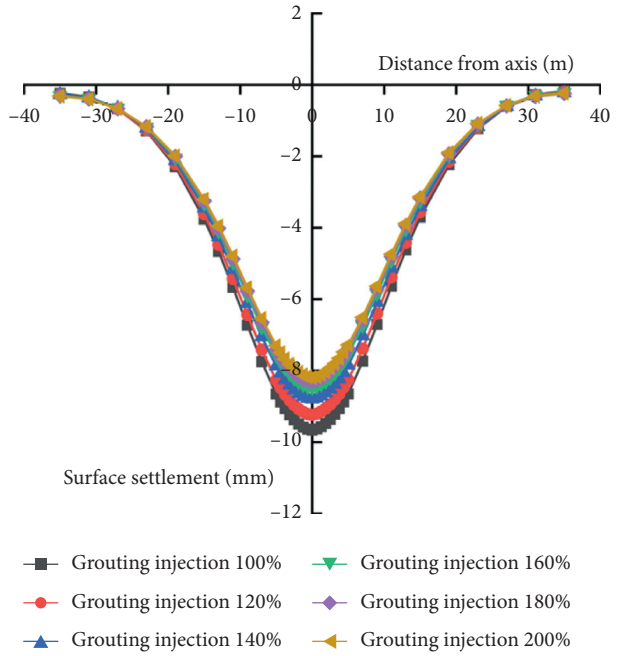

Figure 13: Surface settlement under different grout injection rate conditions.

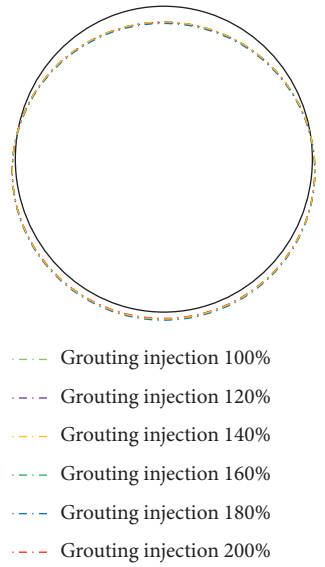

Figure 14: Segment deformation under different grout injection rate conditions.

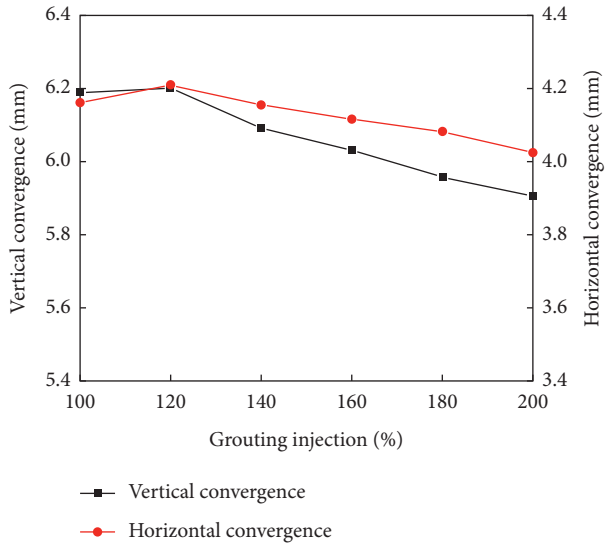

Figure 15: Variation of the convergence value of the segment under different grout injection rate conditions.

decreases. The ellipticity of the segment increases and then decreases with the increase of grout injection rate. When the grout injection rate is 120%, the vertical convergence and horizontal convergence of the segment reach the maximum.

6. Conclusions

(1) The mineral composition of silty clay in the shield muck is mainly composed of quartz (16.38%), feldspar (21.35%), and montmorillonite (31.03%). The mineral composition of fine sand mainly consists of quartz (35.03%) and feldspar (27.35%). It is feasible to use the silty clay and fine sand in shield muck to replace the bentonite and fine sand in raw materials of synchronous grouting, respectively.

(2) Based on the uniform test results, the SPSS multiple regression analysis and MATLAB are used to solve the nonlinear programming problem. The optimal proportions of shield muck synchronous grouting material are water-cement ratio of 0.74, binder-sand ratio of 0.84, bentonite-water ratio of 0.11, and fly ash-cement ratio of 2.75.

(3) The finite difference method is used to analyze the influences of the grouting pressure and the filling rate by considering the combined action of the seepage field, the stress field, and the time-dependent properties of the grout. From the perspective of calculation results and economic benefits, when the grouting pressure is constraint at 0.18 MPa and the grouting rate is arranged at 120%~150%, the surface settlement and the deformation of the segment are better controlled when muck grout is adopted.

Data Availability

The data used to support the findings of this study are available from the corresponding author upon request.

Conflicts of Interest

The authors declare that they have no conflicts of interest.

Acknowledgments

This work was sponsored by the State Key Program of National Natural Science of China (no. 51938005). The authors are grateful to this institution for the support.

References

[1] X. Zha, X. Liao, X. Zhao, F. Liu, A. Q. He, and W. X. Xiong, "Turning waste drilling fluids into a new, sustainable soil resources for landscaping," *Ecological Engineering*, vol. 121, no. 1, pp. 130–136, 2018.

[2] C.-S. Shon, C. K. Estakhri, D. Lee, and D. Zhang, "Evaluating feasibility of modified drilling waste materials in flexible base course construction," *Construction and Building Materials*, vol. 116, pp. 79–86, 2016.

[3] A. Whitaker, C. Penn, and J. Warren, "Surface application of a saline-sodic oil & gas drilling waste to winter wheat (*Triticum aestivum* L.)," *Geoderma*, vol. 274, pp. 97–103, 2016.

[4] Y. Dong, *Study on Solidification Treatment Technology of Waste Drilling Mud*, Chang ' an University, Xian, China, 2009.

[5] Y. Peng, Y. Xu, and C. Sun, "The overview of the way to recycle municipal domestic refuse," *Environmental science and management*, vol. 32, no. 4, pp. 102–104, 2007.

[6] H. Grohs, "Cost-efficient regeneration of bore slurry for driving of weser tunnel," *Tunnel Construction*, vol. 27, no. 6, pp. 47–51, 2007.

[7] X. Zhong, Z. Jia, Q. Liu, and Y. W. Han, "Reuse of excavated fine sand for back grouting of shield tunneling," in *Proceedings of the The 5th National Symposium on Geotechnical Engineering*, Iran, Tehran, December 2008.

[8] L. He, M. Xiao, L. Deng, Y. Liang, and Q. Ding, "Development and application of grouting material with shielded sediment and industrial residue," *The World of Building Materials*, vol. 36, no. 1, pp. 1–5, 2015, (in chinese).

[9] R. K. Rowe, K. Y. Lo, and G. J. Kack, "A method of estimating surface settlement above tunnels constructed in soft ground," *Canadian Geotechnical Journal*, vol. 20, no. 1, pp. 11–22, 1983.
[10] F. Ye, C. Gou, Z. Chen, and J. H. Mao, "Ground surface deformation caused by synchronous grouting of shield tunnels," *Chinese Journal of Geotechnical Engineering*, vol. 36, no. 4, pp. 618–624, 2014.
[11] J. Zhang, T. Feng, J. Yang, F. Yang, and Y. Gao, "Upper-bound finite-element analysis of characteristics of critical settlement induced by tunneling in undrained clay," *International Journal of Geomechanics*, vol. 18, no. 9, Article ID 04018110, 2018.
[12] J. Zhang, T. Feng, J. Yang, F. Yang, and Y. Gao, "Upper-bound stability analysis of dual unlined horseshoe-shaped tunnels subjected to gravity," *Computers and Geotechnics*, vol. 97, pp. 103–110, 2018.
[13] H. Feng and X. Chang, "Analysis of structural disasters in shield tunnels and measures and suggestions for waterproofing," *Modern tunnelling technology*, vol. 53, no. 6, pp. 36–43, 2016.
[14] F. Wang, Y. Fan, and C. Guo, "Practice of non-water-reacting polymer grouting treatment to seepage," *Journal of Hydroelectric Engineering*, vol. 37, no. 10, pp. 1–11, 2018.
[15] P. Song, J. Wang, and Y. Zhou, "Properties of high performance synchronous grouting material of water-resistance property and impermeability," *Bulletin of the Chinese Ceramic Society*, vol. 36, no. 2, pp. 438–442+448, 2017.
[16] K. Fang, *Uniform Design and Uniform Design Table*, Science Press, Beijing, China, 1994.
[17] J. Lei, F. Liu, Q. Wang, G. Peng, and Y. Jiang, "Diffusion characteristics and reinforcement mechanics of grouting in non-homogeneous soil strata," *Geotechnical Engineering Journal*, vol. 37, no. 12, pp. 2245–2253, 2015.